Phys. Med. Biol. **58** (2013) 1303–1314 doi:10.1088/0031-9155/58/5/1303

Registration of sliding objects using direction dependent B-splines decomposition*

V Delmon[1,2], S Rit[1,2], R Pinho[2] and D Sarrut[1,2]

[1] CREATIS; CNRS UMR5220; Inserm U1044; INSA-Lyon; Université Lyon 1, Université de Lyon, Villeurbanne, France
[2] Léon Bérard Cancer Center, University of Lyon, F-69373 Lyon, France

E-mail: vivien.delmon@creatis.insa-lyon.fr

Received 22 May 2012, in final form 18 October 2012
Published 7 February 2013
Online at stacks.iop.org/PMB/58/1303

Abstract
Sliding motion is a challenge for deformable image registration because it leads to discontinuities in the sought deformation. In this paper, we present a method to handle sliding motion using multiple B-spline transforms. The proposed method decomposes the sought deformation into sliding regions to allow discontinuities at their interfaces, but prevents unrealistic solutions by forcing those interfaces to match. The method was evaluated on 16 lung cancer patients against a single B-spline transform approach and a multi B-spline transforms approach without the sliding constraint at the interface. The target registration error (TRE) was significantly lower with the proposed method (TRE = 1.5 mm) than with the single B-spline approach (TRE = 3.7 mm) and was comparable to the multi B-spline approach without the sliding constraint (TRE = 1.4 mm). The proposed method was also more accurate along region interfaces, with 37% less gaps and overlaps when compared to the multi B-spline transforms without the sliding constraint.

(Some figures may appear in colour only in the online journal)

1. Introduction

Image registration is increasingly being used in medical image processing to compare images from different modalities and to account for deformation during or between exams. Common techniques search for the mapping function that minimizes a similarity measure between a reference image and a target image deformed by the mapping function. The problem is known to be ill-posed and a regularization is required to find a physically plausible motion field, e.g., by using smoothness constraints to avoid solutions with large local variations.

However, anatomical regions that slide along each other lead to difficulties in the estimation of the real displacement because the motion is not smooth where sliding occurs. This

* This work was presented in part at the 4th International Workshop on Pulmonary Image Analysis during the Medical Image Computing and Computer Assisted Intervention (MICCAI) in Toronto, Canada (2011).

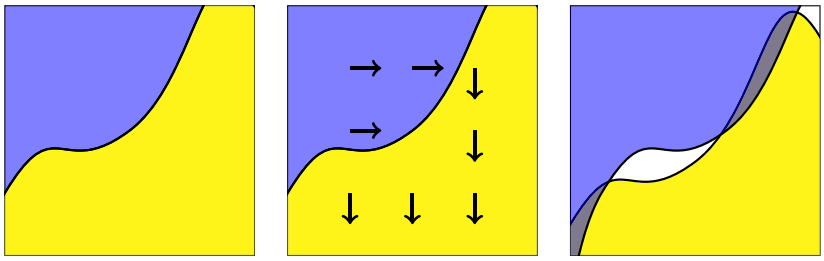

(a) Labels (b) Vector field (c) Forward warp

Figure 1. Illustration of potential issues at a sliding interface when using independent deformation transforms for each regions. The resulting deformation can lead to gaps (white) and overlaps (dark blue).

is the case with the breathing motion, since the pleura allows sliding of the lung parenchyma along the thoracic cage (Wu *et al* 2008). In this case, the smoothness constraint prevents physiologically plausible motions.

Several approaches have been proposed to handle this known problem. The regularization has been adapted to allow discontinuities in certain regions based on the data intensities, while preserving smooth deformations in most regions (Ruan *et al* 2008, Wolthaus *et al* 2008). These regularizations are based on the intensities of the CT image, making them sensitive to noise and inadequate where intensities are similar on both sides of the region interface, e.g., around the liver. Ruan *et al* (2009) improved their regularization term by allowing discontinuities, but penalizing divergent ones in order to prevent local vacuums or mass collisions.

Other approaches (Kabus *et al* 2009, Werner *et al* 2009, Wu *et al* 2008) are based on the segmentation of areas that slide along each other. For example, Kabus *et al* (2009) compared different approaches in which the segmentation of the lungs is used to register each region separately and to allow a discontinuity at their interface. This solution gives better results compared to a single registration, but it does not guaranty consistency between the deformations of each region, allowing gaps and overlaps near the border (figure 1). This consistency constraint is a useful information which could help the registration in regions with poor contrast, e.g., in the lungs where the border region is more homogeneous due to small bronchi less visible on CT images. To constrain alignment, an artificial band can be added around the interface of the registered region in the reference and the target images, in order to guide registration with a strong spatial gradient (Werner *et al* 2009, Wu *et al* 2008). This solution forces the segmentation of both the fixed and the target image and as a result increases the impact of bad or inconsistent segmentations.

Recently, Schmidt-Richberg *et al* (2011) proposed a direction dependent regularization. They separately considered the normal and tangential regularization components according to the boundary of the sliding regions. The normal-directed regularization prevents gaps and overlaps and the tangential regularization allows sliding motion. The segmentation of the sliding regions is still required, but only on the reference image, therefore avoiding the problems of segmentation inconsistencies of previous approaches.

B-spline transforms are among the most popular parametric methods to represent non-rigid deformations, as it has recently been observed in a registration challenge (Murphy *et al* 2011). Part of their success comes from their useful properties, e.g., local support and analytic differentiability. However, they are inherently smooth and their use for sliding motion estimation is not straightforward. To the authors' knowledge, the solution proposed by Wu *et al* (2008) is the only one constraining sliding motion with B-spline transforms. However,

it requires consistent segmentations of the pair of registered images which can be practically difficult to obtain. The purpose of this paper is to propose a linear combination of B-spline transforms to represent a mapping function for the estimation of sliding deformations. The resulting function allows sliding, while preserving the consistency of the interface after warping each region. We have validated our approach by registering 16 publicly available 4D CT data sets of thoracic cancer patients.

2. Method

2.1. Sliding motion properties

Sliding motion occurs when two regions move discontinuously along their interface, but stay in contact with each other. Since a B-spline transform cannot represent such a discontinuous motion, we use one B-spline transform per region, as in previous work (Vandemeulebroucke *et al* 2011, Wu *et al* 2008). Thus, we enforce smoothness in each region, but allow for a discontinuity at their interface.

However, there is no constraint on the consistency of the deformation across the interface, which could potentially lead to gaps and overlaps (figure 1). In sliding deformations, the speed of the displacement is continuous in the direction normal to the sliding interface, simply referred to as the *normal direction* in the following. This constraint was first expressed by Schmidt-Richberg *et al* (2011), who added a local regularity constraint around the sliding interface. In practice, since we have two images acquired at distant time points, the speed direction is approximated by the direction of the deformation between these two time points. This approximation is only valid if the normal direction does not change during the displacement, limiting the approach to planar interfaces moving by translation (Yin *et al* 2010). Nevertheless, when the interface smoothness is large compared to the amplitude of its deformation, the approximation is locally valid. This has been considered the case in the application investigated in this paper, i.e. the estimation of lung sliding motion from 4D CT images.

To express the constraint along the normal direction using B-spline transforms, we propose to add a third B-spline transform to handle the motion in the normal direction on the entire image. Since a B-spline transform can only represent continuous deformations, smoothness in the normal direction is naturally enforced by the proposed model. The next section describes how to decompose the mapping function in these three B-spline transforms for deformable registration of sliding regions.

2.2. Mapping function

The proposed model can handle any number of regions but to simplify the presentation, we consider two complementary regions $\Omega, \overline{\Omega} \in \mathbb{R}^3$ sliding along their interface. The mapping function $\boldsymbol{T} : \Omega \cup \overline{\Omega} \mapsto \mathbb{R}^3$ maps points of the reference image to points of the target image.

Let $\boldsymbol{B}^N, \boldsymbol{B}^{\Omega}, \boldsymbol{B}^{\overline{\Omega}} : \Omega \cup \overline{\Omega} \mapsto \mathbb{R}^3$ be the three B-spline transforms described in the previous section. $\boldsymbol{B}^N$ is the deformation in the normal direction for the whole transformation support $\Omega \cup \overline{\Omega}$. $\boldsymbol{B}^{\Omega}$ and $\boldsymbol{B}^{\overline{\Omega}}$ describe the rest of the deformation in Ω and $\overline{\Omega}$, respectively. The expression of the resulting mapping function is

$$\boldsymbol{T}(\boldsymbol{x}) = \begin{cases} \boldsymbol{B}^N(\boldsymbol{x}) + \boldsymbol{B}^{\Omega}(\boldsymbol{x}) & \text{if } \boldsymbol{x} \in \Omega, \\ \boldsymbol{B}^N(\boldsymbol{x}) + \boldsymbol{B}^{\overline{\Omega}}(\boldsymbol{x}) & \text{if } \boldsymbol{x} \in \overline{\Omega}. \end{cases} \tag{1}$$

Thus, potential inconsistencies between the deformations in Ω and $\overline{\Omega}$ are prevented because the motion in the normal direction is continuously represented by $\boldsymbol{B}^N$, while sliding is possible

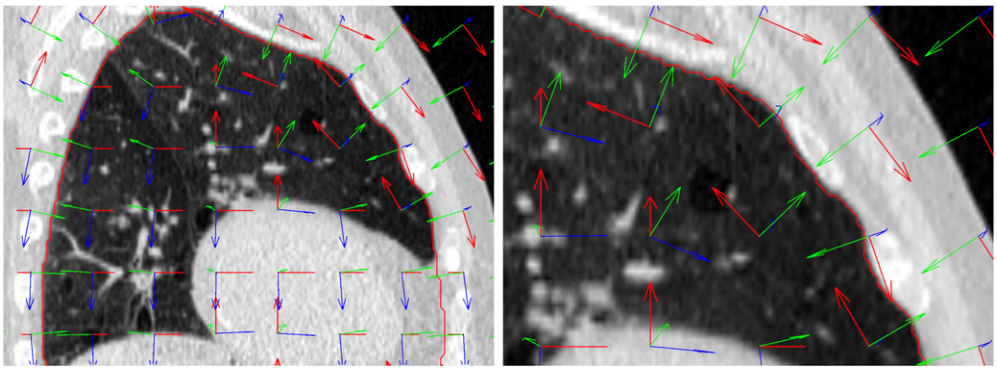

Figure 2. Local bases $\{\boldsymbol{N}(l(\boldsymbol{i})), \boldsymbol{U}(l(\boldsymbol{i})), \boldsymbol{V}(l(\boldsymbol{i}))\}$ superimposed on the corresponding sagittal CT slice of a thorax. $\boldsymbol{N}$, $\boldsymbol{U}$ and $\boldsymbol{V}$ are in green, red and blue, respectively.

because the rest of the transform is separated into two independent B-spline transforms, $\boldsymbol{B}^{\Omega}$ and $\boldsymbol{B}^{\overline{\Omega}}$.

2.3. Parameterization

The B-spline transforms $\boldsymbol{B}^{N}$, $\boldsymbol{B}^{\Omega}$ and $\boldsymbol{B}^{\overline{\Omega}}$ are defined on the same set of control points with their respective B-spline coefficients $\boldsymbol{c}_i^{N}, \boldsymbol{c}_i^{\Omega}, \boldsymbol{c}_i^{\overline{\Omega}} \in \mathbb{R}^3$, e.g., for $\boldsymbol{B}^{\overline{\Omega}}$,

$$\boldsymbol{B}^{\overline{\Omega}}(\boldsymbol{x}) = \sum_{\boldsymbol{i} \in \boldsymbol{J}} \boldsymbol{c}_i^{\overline{\Omega}} \boldsymbol{\beta}_{\boldsymbol{i}}(\boldsymbol{x}), \tag{2}$$

with $\boldsymbol{x} \in \Omega \cup \overline{\Omega}$, $\boldsymbol{i} \in \boldsymbol{J} \subset \mathbb{Z}^3$ the spatial indices of the B-spline control points and $\boldsymbol{\beta}_{\boldsymbol{i}}$ the tensor product of one-dimensional cubic B-spline kernels, $\boldsymbol{\beta}_{\boldsymbol{i}} = \prod_j^3 \beta_i^j$.

Each B-spline transform must be constrained to represent motion in selected directions only. This is achieved by constraining their coefficients $\boldsymbol{c}_{\boldsymbol{i}}$ to lie in a local orthonormal base, the first direction of which is the normal direction, formally denoted $\boldsymbol{N} : \Omega \cup \overline{\Omega} \rightarrow \mathbb{R}^3$ (figure 2). The computation of this local base is detailed in the following section. The coefficients $\boldsymbol{c}_{\boldsymbol{i}}$ represent the 3D displacement of the control point $\boldsymbol{i}$ at position $l(\boldsymbol{i})$ with $l : \boldsymbol{J} \mapsto \Omega \cup \overline{\Omega}$ the function returning the initial location of each control point. We assumed that if control points move in the normal direction, the resulting deformation is in the normal direction, i.e. $\boldsymbol{c}_i^{N} \times \boldsymbol{N}(l(\boldsymbol{i})) = \boldsymbol{0} \Rightarrow \boldsymbol{B}^{N}(\boldsymbol{x}) \times \boldsymbol{N}(\boldsymbol{x}) = \boldsymbol{0}, \forall \boldsymbol{i} \in \boldsymbol{J}, \forall \boldsymbol{x} \in \Omega \cup \overline{\Omega}$. This assumption is only valid for planar sliding interfaces. This is not the case here but the sliding interface is sufficiently smooth to minimize the effect of the resulting approximation. In order to have $\boldsymbol{c}_i^{N} \times \boldsymbol{N}(l(\boldsymbol{i})) = \boldsymbol{0}$, a single parameter $p_i^{N} \in \mathbb{R}$ is sufficient to determine the 3D vector $\boldsymbol{c}_i^{N}$ with

$$\boldsymbol{c}_i^{N} = p_i^{N} \boldsymbol{N}(l(\boldsymbol{i})) \tag{3}$$

Similarly, the control points of $\boldsymbol{B}^{\Omega}$ and $\boldsymbol{B}^{\overline{\Omega}}$ are constrained to vary in a plane orthogonal to $\boldsymbol{N}$, which is supported by the rest of the local orthonormal base defined in each control point (figure 2). For these B-spline transforms two parameters are necessary for each control points. The first one is multiplied by the second vector of the local orthonormal base, $\boldsymbol{U}$, and the second by the third vector of the local orthonormal base, $\boldsymbol{V}$, giving

$$\begin{cases} \boldsymbol{c}_i^{\Omega} = p_i^{\Omega,U} \boldsymbol{U}(l(\boldsymbol{i})) + p_i^{\Omega,V} \boldsymbol{V}(l(\boldsymbol{i})) \\ \boldsymbol{c}_i^{\overline{\Omega}} = p_i^{\overline{\Omega},U} \boldsymbol{U}(l(\boldsymbol{i})) + p_i^{\overline{\Omega},V} \boldsymbol{V}(l(\boldsymbol{i})). \end{cases} \tag{4}$$

Solving the registration problem with the proposed mapping function to represent sliding motion comes down to estimating the optimal parameters p_i^{N}, $p_i^{\Omega,U}$, $p_i^{\Omega,V}$, $p_i^{\overline{\Omega},U}$, and

$p_i^{\overline{\Omega},V}$ that minimize a chosen similarity metric depending on the three constrained B-spline transformations. Subsequently, the final transformation $\boldsymbol{T}$ can be derived from equations (1)–(4).

2.4. Local orthonormal bases

The computation of an orthonormal base $\{\boldsymbol{N}(l(\boldsymbol{i})), \boldsymbol{U}(l(\boldsymbol{i})), \boldsymbol{V}(l(\boldsymbol{i}))\}$ is required at each control point of the B-spline grid (figure 2). $\boldsymbol{N}(l(\boldsymbol{i}))$, is obtained with the derivative of the distance map with respect to the closest interface. In order to prevent aliasing, it was smoothed by a Gaussian filter with a kernel radius of 4 mm radius. $\boldsymbol{U}(l(\boldsymbol{i}))$ and $\boldsymbol{V}(l(\boldsymbol{i}))$ can be any couple of orthogonal vector in the plane orthogonal to $\boldsymbol{N}(l(\boldsymbol{i}))$. We use the cross product between $\boldsymbol{N}(l(\boldsymbol{i}))$ and an arbitrary vector $\hat{\boldsymbol{w}}_{\boldsymbol{i}} \in \mathbb{R}^3$ to obtain $\boldsymbol{U}(l(\boldsymbol{i}))$, followed by a cross product between $\boldsymbol{N}(l(\boldsymbol{i}))$ and $\boldsymbol{U}(l(\boldsymbol{i}))$ to obtain $\boldsymbol{V}(l(\boldsymbol{i}))$. To prevent numerical instabilities, the vector $\hat{\boldsymbol{w}}_{\boldsymbol{i}}$ is the unit vector of the Cartesian basis $\{\boldsymbol{e_x}, \boldsymbol{e_y}, \boldsymbol{e_z}\}$ which forms the largest angle α with $\boldsymbol{N}(l(\boldsymbol{i}))$, $\alpha \in [0, \frac{\pi}{2}]$, i.e.

$$\hat{\boldsymbol{w}}_{\boldsymbol{i}} = \underset{\boldsymbol{w} \in \{\boldsymbol{e_x}, \boldsymbol{e_y}, \boldsymbol{e_z}\}}{\operatorname{argmin}} \|\boldsymbol{N}(l(\boldsymbol{i})) \cdot \boldsymbol{w}\| \tag{5}$$

2.5. Partial derivatives for optimization

Registration is the maximization of a cost function based on a similarity measure, e.g., the mutual information or the correlation coefficient. Several optimization procedures depend on the partial derivatives of the cost function with respect to the transformation parameters. A major advantage of B-spline transforms is that partial derivatives can be expressed analytically as a linear combination of inferior order B-spline functions. Since the proposed method is a linear combination of B-spline transforms in each region, the analytical derivation is preserved. Thus, the derivation of equation 1 gives the following partial derivative for $\boldsymbol{T}(\boldsymbol{x})$

$$\begin{cases} \frac{\partial \boldsymbol{T}(\boldsymbol{x})}{\partial p_i^N} = \frac{\partial \boldsymbol{B}^N(\boldsymbol{x})}{\partial \boldsymbol{c}_i^N} \cdot \boldsymbol{N}(l(\boldsymbol{i})), \\ \frac{\partial \boldsymbol{T}(\boldsymbol{x})}{\partial p_i^{\Omega,U}} = \frac{\partial \boldsymbol{B}^\Omega(\boldsymbol{x})}{\partial \boldsymbol{c}_i^\Omega} \cdot \boldsymbol{U}(l(\boldsymbol{i})), \\ \frac{\partial \boldsymbol{T}(\boldsymbol{x})}{\partial p_i^{\Omega,V}} = \frac{\partial \boldsymbol{B}^\Omega(\boldsymbol{x})}{\partial \boldsymbol{c}_i^\Omega} \cdot \boldsymbol{V}(l(\boldsymbol{i})), \\ \frac{\partial \boldsymbol{T}(\boldsymbol{x})}{\partial p_i^{\overline{\Omega},U}} = \frac{\partial \boldsymbol{B}^{\overline{\Omega}}(\boldsymbol{x})}{\partial \boldsymbol{c}_i^{\overline{\Omega}}} \cdot \boldsymbol{U}(l(\boldsymbol{i})). \\ \frac{\partial \boldsymbol{T}(\boldsymbol{x})}{\partial p_i^{\overline{\Omega},V}} = \frac{\partial \boldsymbol{B}^{\overline{\Omega}}(\boldsymbol{x})}{\partial \boldsymbol{c}_i^{\overline{\Omega}}} \cdot \boldsymbol{V}(l(\boldsymbol{i})). \end{cases} \tag{6}$$

3. Lung sliding motion

We have evaluated the proposed method on 4D CT images of the thorax displaying large sliding motion of the lungs along the thoracic cage. The evaluation was carried out using the target registration error (TRE), and a quantification of overlaps and gaps near the sliding interface.

3.1. Image data

The evaluation was performed on 4D CT images of the thorax of 16 lung cancer patients. The end-inhale phase (target image) was registered on the end-exhale phase (reference image) (figure 3).

The first six patients were treated at our hospital. The images were acquired with a Brilliance Big Bore 16-slice 4D CT scanner (Philips Medical Systems, Cleveland, OH).

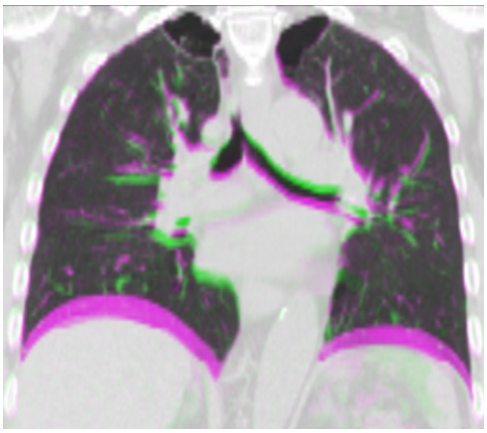

Figure 3. Example of a pair of CT images used for the evaluation of the proposed method. The end-inhale image, in green, is superimposed on the end-exhale image, in purple.

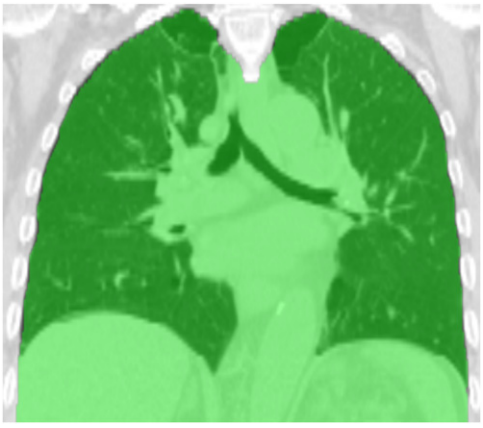

Figure 4. The CT image of a thorax with the motion mask (green) that encompasses the organs with the largest displacement during breathing.

Respiration-correlated reconstruction into ten 3D CT images was obtained by simultaneous recording of a respiratory trace using the Pneumo Chest bellows (Lafayette Instrument, Lafayette, IN). The resolution was approximately $1 \times 1 \times 2$ mm^3 and $512 \times 512 \times 150$ voxels (Vandemeulebroucke *et al* 2011).

The next ten patients were obtained from the DIR-labs (DL) database www.dir-lab.com Castillo *et al* (2009, 2010). Their spatial resolution was between $0.97 \times 0.97 \times 2.5$ and $1.16 \times 1.16 \times 2.5$ mm^3.

3.2. Motion mask segmentation

For each patient the motion mask was extracted on the end-exhale image (figures 3 and 4). The motion mask was first described by Wu *et al* and divides the thorax in two sliding regions (Wu *et al* 2008). The motion mask Ω encompasses the organs with the largest displacements during

breathing, comprising the lung, the mediastinum and the abdomen; the complementary region $\overline{\Omega}$ encompasses the more static organs, comprising the thoracic cage and the backbone. The segmentation was achieved using an automated method (Vandemeulebroucke *et al* 2012) based on an initial segmentation of the lungs (threshold and region growing), the bones (threshold and connected components) and the patient. A monitored level-set segmentation is initialized at the center of the abdomen. The level-set surface then grows into the lungs until 95% of the lung volume is covered, without intersecting the bones. The advantage of this motion mask compared to a simple lung mask is that it encompasses the abdomen and the mediastinum which move continuously with the lungs under the influence of the breathing motion.

3.3. Implementation

The proposed mapping function was implemented as a new component of elastix (release 4.6, available at http://elastix.isi.uu.nl/), which is a toolbox for intensity-based medical image registration (Klein *et al* 2010). We compared the end-inhale to end-exhale registrations of the proposed method with one using a single B-spline transform defined on the whole image, one using two independent B-splines without sliding constraint, one in Ω and another in $\overline{\Omega}$, and, finally, the method described in Wu *et al* (2008) and Vandemeulebroucke *et al* (2012) which models the sliding constraint using a strong gradient defined on both the reference and the target images.

Registration parameters are the same for the four methods. We used third order B-spline transformations optimized with a very large number of iterations (16 000) of the adaptive stochastic gradient descent (Klein *et al* 2009) to guarantee convergence. The spacing of the B-spline control points was 32 mm in every direction, which is large enough to impose spatially smooth deformations without additional regularization. The Mattes mutual information metric (Mattes *et al* 2003) used 2048 voxels which were randomly chosen at every iteration. The moving image was interpolated using third order B-splines. To take into account large deformations, we used a multi-resolution strategy with a smoothing Gaussian kernel on three resolution levels.

3.4. Quantification

Two measures were employed in the evaluation of the results:

(1) TRE. To measure the quality of the registration, we used the mean Euclidean distance between corresponding landmarks defined in the reference image and in the target image. These landmarks correspond to recognizable structures like bronchial tree bifurcations, manually selected by experts, on both the reference and the target image.

For the first six patients, 100 landmarks were obtained with the semiautomatic method described in Vandemeulebroucke *et al* (2011). For DL patients, 300 landmarks were chosen as described in Castillo *et al* (2009, 2010).

The TREs of several registration methods applied to the DL' dataset are available on the DL' website as well as in several publications, e.g., Schmidt-Richberg *et al* (2011).

(2) Gaps and overlaps. To measure the consistency between the deformation fields around the sliding interface, we quantified gap and overlap volumes near the segmentation boundary, because gaps and overlaps at the pleura are physically impossible for healthy subjects. Since the sliding interface was between Ω and $\overline{\Omega}$, the motion mask was converted into a 3D surface mesh, which was deformed using both the transform in Ω ($\boldsymbol{B}^{\Omega} + \boldsymbol{B}^{N}$) and the transform in $\overline{\Omega}$

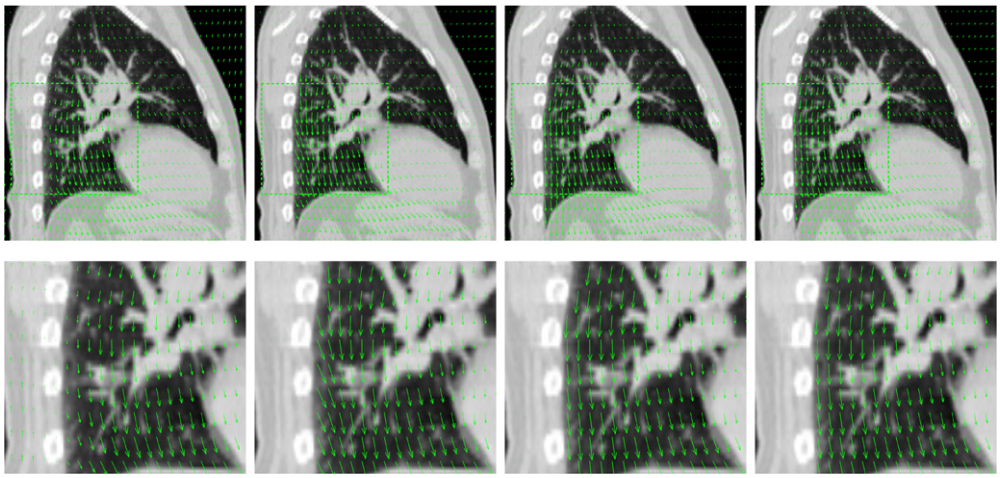

(a) (b) (c) (d)

Figure 5. Example of deformation vector fields obtained after registration using a single B-spline (a), multiple B-spline without sliding constraint (b), Wu *et al* 's method (c) and multiple B-spline with sliding constraint (d).

$(\boldsymbol{B}^{\overline{\Omega}} + \boldsymbol{B}^{N})$. By converting these two meshes back into binary masks, we identified overlap voxels $\boldsymbol{T}(\Omega) \cap \boldsymbol{T}(\overline{\Omega})$ and gap voxels $\overline{\boldsymbol{T}(\Omega)} \cap \overline{\boldsymbol{T}(\overline{\Omega})}$ and measured their total volume in cm^3.

We compared the multi B-spline methods with and without sliding constraint by computing their Jaccard distances, equal to

$$J(A, B) = \frac{|A \cup B| - |A \cap B|}{|A \cup B|} \tag{7}$$

with $A = \boldsymbol{T}(\Omega)$ and $B = \overline{\boldsymbol{T}(\overline{\Omega})}$. Note that the numerator of the Jaccard distance is the union of gap and overlap volumes. The ratio of the Jaccard distances between two method shows the improvement brought by one method on the other one.

4. Results

Figure 5 shows the deformation vector fields obtained with the four methods for one pair of images. The single B-spline transform (figure 5(a)) does not take into account the discontinuity at the motion mask interface, leading to incorrect motion. In that area, the resulting mapping function varies smoothly, leading to a wrong estimate of the motion. The use of one B-spline per area (figure 5(b)) corrects this drawback by preventing the influence of structures outside the motion mask on the estimation of the motion of structures in the motion mask, and conversely. However, it leads to inconsistencies on both sides of the interface. Namely, the B-spline transform inside the motion mask warps the interface inward, while the B-spline transform outside the motion mask warps the interface in the opposite direction, creating gaps (figure 6(a)). Wu *et al* 's method and the proposed method (figures 5(c) and (d)) achieve accurate estimation of sliding motion, additionally constraining the estimated motion to be consistent around the sliding interface, reducing gaps and overlaps (figures 6(b) and (c)).

In table 1, we observed that handling the sliding motion discontinuity with multiple B-spline transforms improves the resulting TRE (average reduction from more than 3.7 mm to about 1.4 mm). This result confirmed previous studies (Schmidt-Richberg *et al* 2011, Vandemeulebroucke *et al* 2012, Wu *et al* 2008). A two-sample *t*-test showed that the TRE

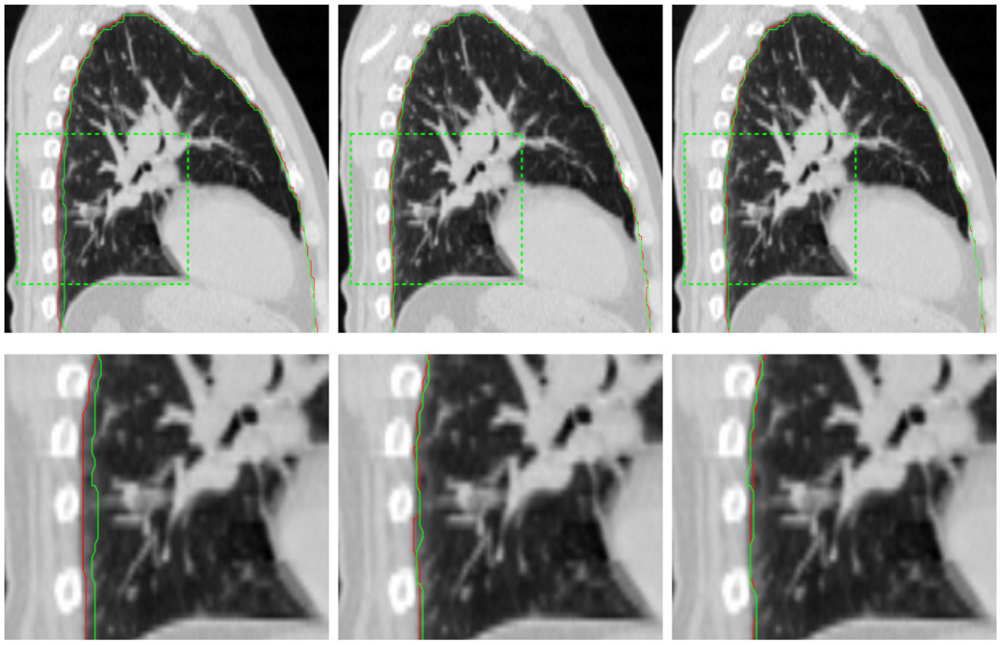

(a) (b) (c)

Figure 6. The motion mask interface deformed with the inside deformation (green) and the outside deformation (red) using one B-spline per region (a), using Wu *et al* 's method (b) and using the proposed method (c).

Table 1. TRE after three resolutions (in mm).

Patient	Before	Single B-spline	Multi B-splines without sliding constraint	Multi B-splines Wu *et al* (2008)	Multi B-splines with sliding constraint
1	9.4 ± 7.4	2.2 ± 2.6	1.2 ± 1.2	1.2 ± 1.1	1.2 ± 1.3
2	7.3 ± 4.9	2.6 ± 3.1	1.5 ± 1.8	1.4 ± 2.1	1.6 ± 1.9
3	7.1 ± 5.1	2.0 ± 2.2	1.3 ± 0.8	1.2 ± 0.7	1.3 ± 0.8
4	6.7 ± 3.7	1.6 ± 1.6	1.0 ± 0.6	1.0 ± 0.5	1.0 ± 0.6
5	14.0 ± 7.2	5.2 ± 5.5	1.3 ± 1.0	1.3 ± 1.0	1.4 ± 1.0
6	6.3 ± 2.9	1.3 ± 0.9	0.9 ± 0.5	0.8 ± 0.4	0.9 ± 0.5
DL 1	3.9 ± 2.8	1.7 ± 1.1	1.3 ± 0.6	1.1 ± 0.5	1.2 ± 0.6
DL 2	4.3 ± 3.9	1.9 ± 1.9	1.0 ± 0.5	1.0 ± 0.5	1.1 ± 0.6
DL 3	6.9 ± 4.1	3.3 ± 2.5	1.7 ± 0.9	1.3 ± 0.7	1.6 ± 0.9
DL 4	9.8 ± 4.9	3.3 ± 2.7	1.6 ± 1.1	1.5 ± 1.0	1.6 ± 1.1
DL 5	7.5 ± 5.5	4.1 ± 3.6	1.9 ± 1.5	1.9 ± 1.5	2.0 ± 1.6
DL 6	10.9 ± 7.0	5.0 ± 4.4	1.6 ± 0.9	1.6 ± 0.9	1.7 ± 1.0
DL 7	11.0 ± 7.4	7.0 ± 6.4	1.7 ± 1.1	1.7 ± 1.1	1.9 ± 1.2
DL 8	15.0 ± 9.0	10.5 ± 9.3	1.8 ± 1.7	1.6 ± 1.4	2.2 ± 2.3
DL 9	7.9 ± 4.0	4.3 ± 2.9	1.5 ± 0.8	1.4 ± 0.8	1.6 ± 0.9
DL 10	7.3 ± 6.3	3.9 ± 4.4	1.6 ± 1.2	1.6 ± 1.2	1.7 ± 1.2
mean	8.4 ± 5.6	3.7 ± 4.0	1.43 ± 1.1	1.35 ± 1.0	1.49 ± 1.2

obtained with multiple B-spline methods significantly improved the TRE obtained with the single B-spline method ($p < 0.001$, paired t-test). Nevertheless, our method yielded slightly worse results when compared with the multi B-splines method without sliding constraint.

Table 2. Gaps and overlaps volumes (in cm^3) followed by the Jaccard distance ratio between both methods.

Patient	Multi B-splines without sliding constraint		Multi B-splines Wu *et al* (2008)		Multi B-splines with sliding constraint	
	Gaps	Overlaps	Gaps	Overlaps	Gaps	Overlaps
1	120	62	77	59	76	57
2	154	47	72	62	82	51
3	100	37	72	31	62	33
4	158	68	101	58	78	64
5	337	75	145	84	134	100
6	157	69	108	48	72	59
DL 1	66	9	38	26	39	15
DL 2	83	55	78	46	67	60
DL 3	220	15	99	28	83	33
DL 4	102	30	75	34	66	44
DL 5	140	40	110	38	78	52
DL 6	282	66	100	86	119	77
DL 7	247	56	105	79	108	77
DL 8	201	94	96	91	92	93
DL 9	105	35	61	34	54	44
DL 10	202	56	120	63	94	56
mean	167 ± 76	51 ± 22	91 ± 26	54 ± 22	82 ± 24	57 ± 22

The TRE increased by 0.06 mm on average ($p \simeq 0.03$). We specifically evaluated the set of landmarks which are less than 5 mm away from the motion mask boundary. The TRE was 2.86, 1.22, 1.23 and 1.29 mm for the single B-spline, multiple B-Spline, Wu *et al* 's method and multiple B-spline with sliding constraint, respectively. However, the set of points near the boundary is limited to 13.5 points per patient on average, due to the lack of anatomical landmarks near the boundary. The gaps and overlaps measure is more descriptive of the sliding pleurae.

The proposed method improved the registration at the interface by significantly decreasing gap volumes from 167 to 56 cm^3 ($p < 10^{-3}$) (table 2). These gaps are due to the lack of structures in the lungs near the thoracic wall, which let the registration rely on internal structures for aligning the pleura. With the sliding constraint, the two motions masks are visually interlaced (figure 6), which also resulted in a minor 6 cm^3 increase of the overlaps. The combined measurement, the Jaccard distance ratio, was always in favor of the proposed method with an average improvement of 34%.

In terms of computation time (16 000 iterations, 2048 samples, 32 mm spacing, three resolutions), the single B-spline method took around 48 min, the multi B-spline method took around 58 min, Wu *et al* 's method took 100 min (48 min for the inside of the motion mask and 52 min for the outside) and the proposed method took around 86 min on an Intel Xeon E5345 @ 2.33 GHz. The computation time of the multi B-spline method was 21% longer than the single B-spline method because the second B-spline doubles the number of considered parameters. The proposed method was 79% slower than the single B-spline method, which is due to the initial normal vector field computation, the local base computation at each resolution, as well as per-iteration costs, such as the parameters dispatch between each underlying B-spline transform and the cost involved at each deformation evaluation or derivative evaluation to aggregate results of underlying B-spline transforms. The registration time can be reduced a lot by decreasing the number of iterations but we wanted to ensure complete convergence. In practice, we experienced convergence around 2000 iterations, where the proposed elastix implementation takes less than 15 min to perform the registration.

5. Discussion

The results obtained in our evaluation show the interest of taking into account the sliding effect present in the breathing motion when registering images of the lungs. The TRE was comparable when we used an independent B-spline transform for each sliding region but the proposed method significantly reduced inconsistencies along the interface (tables 1 and 2). This means that enforcing continuity of the normal direction gives more plausible deformation fields.

The consistency of the deformation field in methods that use independent transforms can be improved with the inclusion of an artificial band around each region, which creates a strong gradient along the borders and forces their alignment (Vandemeulebroucke *et al* 2012, Wu *et al* 2008). However, these methods must correctly segment both the reference and the target images, so that region borders correspond. In case of segmentation errors, borders which do not represent the same physical structure are wrongly forced to map. The proposed method, on the other hand, requires the segmentation of the fixed image only, lowering the impact of an erroneous segmentation. There is also an advantage for spatio-temporal motion estimation (Vandemeulebroucke *et al* 2011) because the proposed method requires only one segmentation, while other approaches need as many consistent motion masks as image phases. This would be particularly useful in clinical practice, since asking a clinician to review one mask is possible, but reviewing ten masks is not, especially if inter-consistency must be checked.

One limitation of the proposed method is that it cannot handle the sliding on curved borders since, in this case, the normal direction is changing during the displacement. However, if the motion amplitude is small with respect to the curvature, the variation of the normal direction during the deformation is limited and can be neglected. The breathing motion corresponds to such a favorable situation because the sliding border of the lungs is smooth except in the upper part of the lungs where the motion amplitude is small. The approximation might still explain the slight deterioration of the TRE with the sliding constraint (table 1). Registering intermediate images of the breathing cycle could reduce the approximation since they correspond to motion of smaller magnitude. Another potential improvement of the method would be its combination with a spatio-temporal model to access a continuous representation of the deformation in time (Vandemeulebroucke *et al* 2011).

Another limitation comes from the use of a B-spline transform to represent the normal direction. In the proposed solution, only the control points of this B-spline transform are constrained to move in the normal direction, assuming that the resulting transform will also vary in the normal direction. But the displacement at each point of a B-spline transform is the linear combination of the displacement of several control points in a local support, and the assumption is only valid if the normal direction is smooth enough in this local support. The spacing of the control points must therefore be adapted to the smoothness of the interface. 32 mm spacing was deemed adequate in our case. Note that further reducing the grid spacing would also reduce the intrinsic regularity of the B-spline transform and would probably require an additional spatial regularization. Adding a regularization based on the spatial partial derivatives of the transformation, e.g., the bending energy, is straightforward given the analytical derivation of the proposed transform (equation (6)). Our solution preserves indeed the good properties of the B-spline transforms since it is a linear combination of B-spline transforms (equation (1)).

6. Conclusion

We have proposed a mapping function that model sliding motion using a linear combination of multiple B-spline transforms to produce more consistent deformation vector fields compared

to previous approaches. The mapping function has been validated on 16 thorax CT images with lung sliding motion. Compared to previous approaches, we suppressed the need for multiple consistent segmentations while largely reducing gaps and overlaps at interfaces between objects.

Acknowledgments

This work was supported in part by the Labex PRIMES (ANR), the Lyric grant INCa-4664, the Association Nationale de la Recherche Technique (ANRT) and Elekta.

References

Castillo E, Castillo R, Martinez J, Shenoy M and Guerrero T 2010 Four-dimensional deformable image registration using trajectory modeling *Phys. Med. Biol.* **55** 305

Castillo R, Castillo E, Guerra R, Johnson V E, McPhail T, Garg A K and Guerrero T 2009 A framework for evaluation of deformable image registration spatial accuracy using large landmark point sets *Phys. Med. Biol.* **54** 1849

Kabus S, Klinder T, Murphy K, van Ginneken B, Lorenz C and Pluim J P W 2009 Evaluation of 4D-CT lung registration *MICCAI '09: Proc. 12th Int. Conf. on Medical Image Computing and Computer-Assisted Intervention: Part 1 (London, UK)* pp 747–54

Klein S, Pluim J, Staring M and Viergever M 2009 Adaptive stochastic gradient descent optimisation for image registration *Int. J. Comput. Vis.* **81** 227–39

Klein S, Staring M, Murphy K, Viergever M and Pluim J 2010 Elastix: a toolbox for intensity-based medical image registration *IEEE Trans. Med. Imaging* **29** 196–205

Mattes D, Haynor D, Vesselle H, Lewellen T and Eubank W 2003 PET-CT image registration in the chest using free-form deformations *IEEE Trans. Med. Imaging* **22** 120–8

Murphy K *et al* 2011 Evaluation of registration methods on thoracic CT: the EMPIRE10 challenge *IEEE Trans. Med. Imaging* **30** 1901–20

Ruan D, Esedoglu S and Fessler J A 2009 Discriminative sliding preserving regularization in medical image registration *Proc. 6th IEEE Int. Conf. on Symp. on Biomedical Imaging: From Nano to Macro* (Piscataway, NJ: IEEE Press) pp 430–3

Ruan D, Fessler J A and Esedo S 2008 Discontinuity preserving regularization for modeling sliding effects in medical image registration *Proc. IEEE Nucl. Sci. Symp. Conf. Rec.* pp 5304–8

Schmidt-Richberg A, Werner R, Handels H and Ehrhardt J 2011 Estimation of slipping organ motion by registration with direction-dependent regularization *Med. Image Anal.* **16** 150–9

Vandemeulebroucke J, Bernard O, Rit S, Kybic J, Clarysse P and Sarrut D 2012 Automated segmentation of a motion mask to preserve sliding motion in deformable registration of thoracic CT *Med. Phys.* **39** 1006

Vandemeulebroucke J, Rit S, Kybic J, Clarysse P and Sarrut D 2011 Spatiotemporal motion estimation for respiratory-correlated imaging of the lungs *Med. Phys.* **38** 166–78

Werner R, Ehrhardt J, Schmidt-Richberg A and Handels H 2009 Validation and comparison of a biophysical modeling approach and non-linear registration for estimation of lung motion fields in thoracic 4D CT data *Proc. SPIE* **7259** 72590U

Wolthaus J, Sonke J-J, van Herk M and Damen E 2008 Reconstruction of a time-averaged midposition CT scan for radiotherapy planning of lung cancer patients using deformable registration *Med. Phys.* **35** 3998–4011

Wu Z, Rietzel E, Boldea V, Sarrut D and Sharp G 2008 Evaluation of deformable registration of patient lung 4DCT with subanatomical region segmentations *Med. Phys.* **35** 775–81

Yin Y, Hoffman E A and Lin C L 2010 Lung lobar slippage assessed with the aid of image registration *MICCAI '10: Int. Conf. on Medical Image Computing and Computer-Assisted Intervention (Lecture Notes in Computer Science* vol 6362*)* ed T Jiang, N Navab, J P Pluim and M A Viergever (Berlin: Springer) pp 578–85 (availabel at http://dl.acm.org/citation.cfm?id=1928047.1928123)